Pergamon

Int. J. Solids Structures Vol. 35, No. 12, pp. 1163–1185, 1998

0020–7683/98 $19.00 + .00

PII: S0020–7683(97)00097–8

IMPROVED THEORETICAL SOLUTIONS FOR ADHESIVE LAP JOINTS

M. Y. TSAI†
Department of Engineering Science and Mechanics, Virginia Polytechnic Institute and State University, Blacksburg, VA 24061-0219, U.S.A.

D. W. OPLINGER
Federal Aviation Administration Technical Center, Atlantic City International Airport, NJ 08405, U.S.A.

and

J. MORTON
Structural Materials Center, Defense Evaluation and Research Agency, Farnborough, Hampshire, GU14 6TD, U.K.

(*Received* 7 *April* 1996; *in revised form* 24 *March* 1997)

Abstract—Improved theoretical solutions for adhesively bonded single- and double-lap joints are proposed. The classical theories of Volkersen/de Bruyne's solution for double-lap joints, Volkersen's, Goland and Reissner's solutions for single-lap joints, which neglect adherend shear deformations, are used as the bases for the present analyses. The assumption of linear shear stress distributions through the thickness of the adherends is adopted in the analyses. The improved solutions are justified by comparing with the original theoretical solutions, and experimental and numerical results. It is shown that the improved solutions provide a better prediction for the adhesive shear distributions and maximum values, particularly in the case of fiber composite adherends. The effects of the adherend shear deformations on the adhesive shear distributions are presented and the relevant parameters are identified and discussed. © 1998 Elsevier Science Ltd.

INTRODUCTION

The use of adhesive bonding joints in load-bearing structures is of great interest to the aerospace and automotive, as well as the wood and plastics industries, as a result of time and cost savings, high corrosion and fatigue resistance, crack retardance and good damping characteristics. In order to satisfy safety and durability requirements, stress analyses have to be conducted in joint design. Stress analyses are readily performed through numerical analyses such as finite element method. However, theoretical analyses are more effective for identifying key parameters.

The development of theoretical models of the adhesive joints has taken over five decades. For single-lap joints, Volkersen (1938) first proposed a simple shear lag model based on the assumption of one-dimensional bar-like adherends with only shear deformation in the adhesive layer. Later, Goland and Reissner (1944) postulated a beam-on-elastic-foundation model, simulating the joint as consisting of two beams bonded with a shear- and transverse normal-deformable adhesive layer. Hart-Smith (1973a) extended the Goland and Reissner model to treat joints with elastic–plastic adhesives. The emergence of the electronic packaging industry has generated additional interest in adhesive bonding technology. Recent contributions from this sector include Suhir (1986, 1989) who provided a beam-like solution for thermal-induced bimetal interfacial stresses by taking into account transverse interfacial compliance of the strips, and Suhir (1994) who provided a theoretical analysis of cylindrical double lap shear joints. Other recent contributions include Delale *et al.* (1981) who developed two-dimensional closed form solutions for bonded joints, and Lin and Lin (1993) who derived a finite element model of single-lap adhesive joints. Oplinger

† Address for correspondence: Tjing Ling Industrial Research Institute, National Taiwan University, 130 Keeling Road, Sec. III, Taipei, Taiwan, Republic of China.

(1994) developed a layered beam theory to investigate the effect of adherend deflection on the adhesive stress distributions. Tsai and Morton (1994) evaluated theoretical solutions using nonlinear finite element analyses, and resolved some controversies and inconsistencies between the theories. Tsai and Morton (1995) also performed experimental analysis to verify the nonlinear deformations of the single-lap joints, and adhesive stress distributions.

De Bruyne (1944) adapted Volkersen's single-lap theory for the double-lap joints (referred to as Volkersen/de Bruyne in the present study). Hart-Smith (1973b) extended the Volkersen/de Bruyne model to include adhesive plasticity and adherend thermal mismatch. Of the above models and analyses, the Volkersen and Goland and Reissner solutions for single-lap joints, and Volkersen/de Bruyne solution for double-lap joints are most widely used.

The objectives of this investigation are to improve the classical solutions of double- and single-lap joints by incorporating with the adherend shear deformations, to verify the proposed theories through comparison with experimental and numerical results, and, finally, to study the effect of adherend shear on the adhesive stress distributions.

ADHEREND SHEAR DEFORMATION

Configurations and deformations of double- and single-lap joints modeled in the classical theoretical solutions are shown in Fig. 1. For the double-lap joint shown in Fig. 1(a), Volkersen/de Bruyne modeled the adherends as the bars which are allowed to deform, in the longitudinal direction, uniformly through the thickness of the adherends. The adhesive layer was considered to be a shear spring carrying only the shear stresses needed to transfer the longitudinal forces from the inner to the outer adherends. For the single-lap joint, Goland and Reissner improved Volkersen's model [in Fig. 1(b)] by treating the adherends as beams, and the adhesive layer as shear plus transverse normal springs, shown in Fig. 1(c).

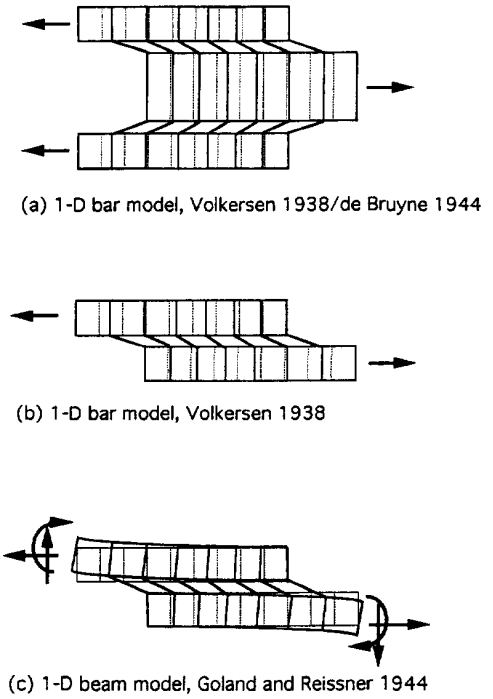

Fig. 1. Configurations and deformations of theoretical models: (a) 1-D bar model (Volkersen, 1938; de Bruyne, 1944) for double-lap joint; (b) 1-D bar model (Volkersen, 1938) for single-lap joint; and (c) 1-D beam model (Goland and Reissner, 1944) for single-lap joint.

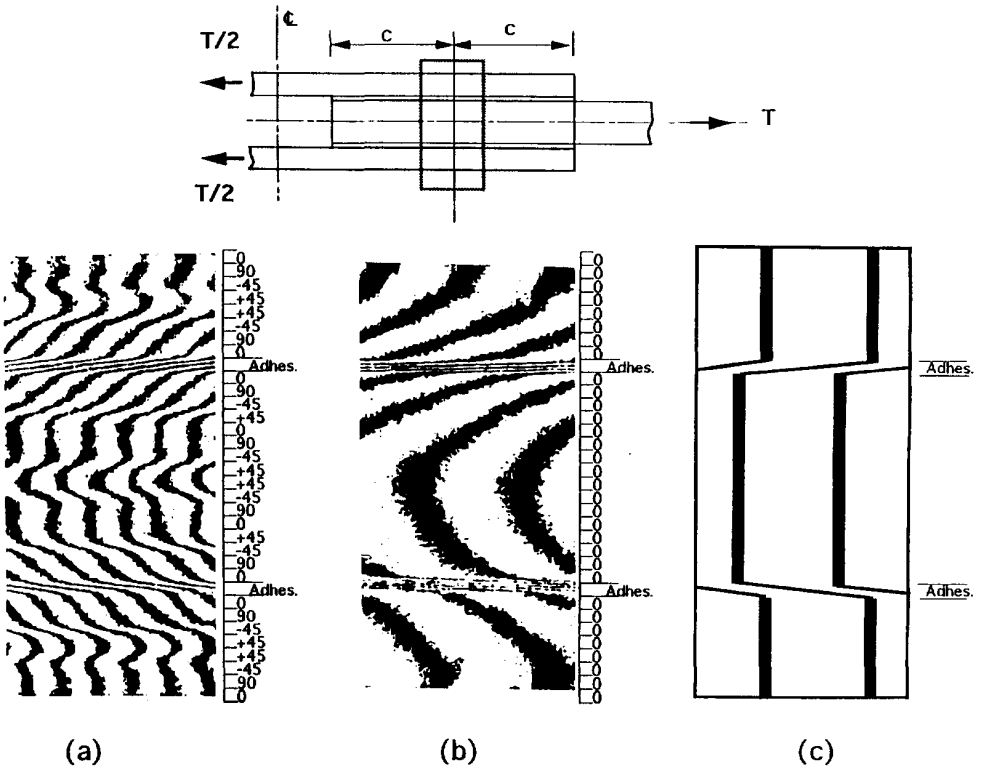

Fig. 2. Experiment (moiré)-determined adherend and adhesive (horizontal) deformations for double-lap joints; (a) with graphite–epoxy quasi-isotropic adherends; (b) with graphite–epoxy unidirectional adherends; (c) adherend and adhesive (horizontal) deformations of theoretical model [1-D bar model (Volkersen, 1938; de Bruyne, 1944)].

Shear deformations in the adherends are ignored (or excluded) in the models mentioned above, possibly due to the relatively small values compared to longitudinal normal deformations in some cases, or due to the complexity of formulations. As mentioned earlier, the adhesive layer can sustain significant shear stresses during load transfer. These large shear stresses would also be present at the adherend surfaces adjacent to the adhesive layer for shear stress equilibrium at the interface. These shear stresses would cause the adherend shear deformations, especially for adherends with relatively low transverse shear modulus such as in the case of laminated composite adherends. Experimental evidence for double-lap joints (Tsai *et al.*, 1996b), shown in Fig. 2, indicates that the longitudinal deformations of the bar- (or beam-) like adherends in theoretical model, in Fig. 2(c), are very different from the case of adherends with significant shear deformations, shown in Fig. 2(a, b). It is noted that Fig. 2(a, b) represents quasi-isotropic ($[0/90/-45/45]_{2s}$) and unidirectional ($[0]_{16}$) laminated composite double-lap joints. Thus, adherend shear deformations should be included in the theoretical models.

Schematics of the deformations of the joints shown in Fig. 3 represent those including adherend shear deformations for double- and single-lap joints. The deformations of the joints in Fig. 3 are more realistic than those in Fig. 1. So that, the associated models will be expected to result in better solutions for analyzing adhesive joints.

DOUBLE-LAP JOINTS

Formulation

Consider a double-lap joint with geometry and material parameters, shown in Fig. 4. The length of the overlap is $2c$. The thicknesses of the outer and inner adherends are t_o and t_i, respectively. E_o and G_o are elastic modulus (in the longitudinal direction) and shear modulus (in the transverse direction) for the outer adherends, and E_i and G_i are the

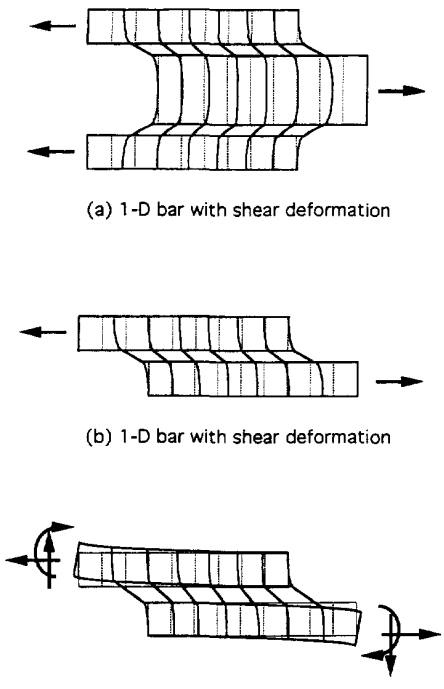

Fig. 3. Configurations and deformations of theoretical models including the shear deformations of adherends: (a) 1-D bar model for double-lap joint; (b) 1-D bar model for single-lap joint; and (c) 1-D beam model for single-lap joint.

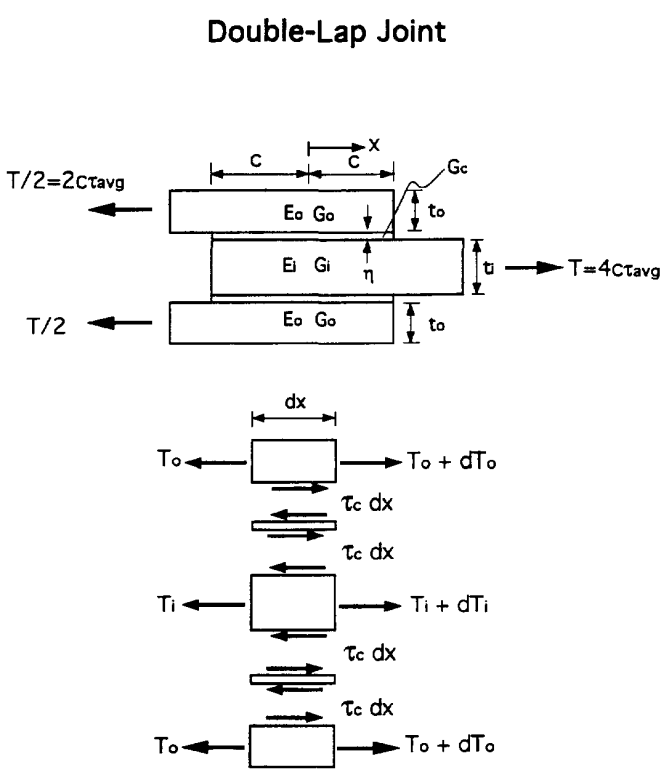

Fig. 4. Geometry and material parameters of the double-lap joint, and an elementary 1-D bar model.

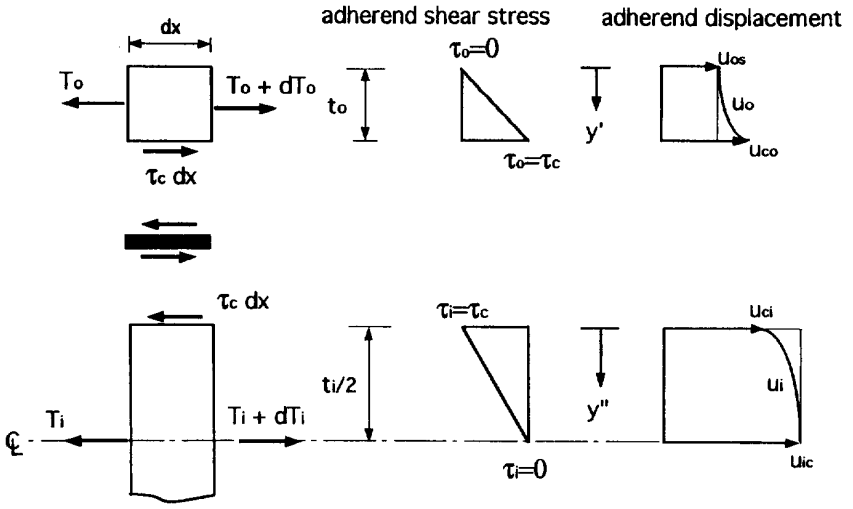

Fig. 5. An assumption of a linear shear stress (strain) distribution through the thickness of adherends.

corresponding properties of the inner adherent. G_c and η are the adhesive shear modulus and thickness. T is an applied force per unit width. T_o and T_i represent longitudinal forces per unit width acting at the outer and inner adherends, respectively. τ_{avg} is the average adhesive shear stress over the bond line. That is:

$$\tau_{avg} = \frac{1}{2c}\int_{-c}^{c} \tau_c \, dx = \frac{T}{4c} \tag{1}$$

where τ_c is adhesive shear stress. Following the notation in Fig. 4, the equilibrium equations for the basic elements of the outer and inner adherends can be written as:

$$\frac{dT_o}{dx} + \tau_c = 0, \tag{2}$$

$$\frac{dT_i}{dx} - 2\tau_c = 0. \tag{3}$$

Shear deformations of the adherends are incorporated by considering the kinematics of the basic elements for the outer and inner adherends are illustrated in Fig. 5. A linear shear stress (strain) distribution through the thickness of the adherend is assumed. Thus, the adherend shear τ_o for the outer adherend and τ_i for the inner adherend can be expressed as

$$\tau_o = \frac{\tau_c}{t_o} y' \tag{4a}$$

and

$$\tau_i = \tau_c \left(1 - \frac{2y''}{t_i}\right) \tag{4b}$$

where y' (y'') is a local coordinate system with the origin at the top surface of the outer (inner) adherend. Equations (4a) and (4b) are based on zero shear stresses at the top surface of the outer adherend (i.e. at $y' = 0$) and at the center of the inner adherend (i.e. at $y'' = t_i/2$), and $\tau_o = \tau_c$ at $y' = t_o$ and $\tau_i = \tau_c$ at $y'' = 0$. Then with a linear material constitutive

relationship the adherend shear strain γ_o for the outer adherend and γ_i for the inner adherend are written as

$$\gamma_o = \frac{\tau_c}{G_o t_o} y' \tag{5a}$$

and

$$\gamma_i = \frac{\tau_c}{G_i}\left(1 - \frac{2y''}{t_i}\right). \tag{5b}$$

The longitudinal displacement functions u_o for the outer adherend and u_i for the inner adherend are given by

$$u_o(y') = u_{os} + \int_0^{y'} \gamma_o(\hat{y}')\,\mathrm{d}\hat{y}' = u_{os} + \frac{\tau_c}{2G_o t_o} y'^2 \tag{6a}$$

and

$$u_i(y'') = u_{ci} + \int_0^{y''} \gamma_i(\hat{y}'')\,\mathrm{d}\hat{y}'' = u_{ci} + \frac{\tau_c}{G_i}\left(y'' - \frac{y''^2}{t_i}\right) \tag{6b}$$

where u_{os} represents the displacement at the top surface of the outer adherend and u_{ci} is the adhesive displacements at the interface between the adhesive and inner adherend. Note that, due to the perfect bonding of the joints, the displacements are continuous at the interfaces between the adhesive and adherends. As a result, the u_{ci} should be equivalent to the inner adherend displacement at the interface and u_{co} (the adhesive displacement at the interface between the adhesive and outer adherend) should be the same as the outer adherend displacement at the interface. Based on eqn (6a), the u_{co} can be expressed as

$$u_{co} = u_o(y' = t_o) = u_{os} + \frac{\tau_c t_o}{2G_o}. \tag{7}$$

Using eqn (7), eqn (6a) can be rewritten as

$$u_o(y') = u_{co} + \frac{\tau_c}{2G_o t_o} y'^2 - \frac{\tau_c t_o}{2G_o}. \tag{6c}$$

The longitudinal resultant forces, T_o and T_i, for the outer and inner adherends, respectively, are

$$T_o = \int_0^{t_o} \sigma_o(y')\,\mathrm{d}y' \tag{8a}$$

and

$$T_i = 2\int_0^{t_i/2} \sigma_i(y'')\,\mathrm{d}y'' \tag{8b}$$

where σ_o and σ_i are longitudinal normal stresses for the outer and inner adherends, respectively. By transforming these stresses into functions of displacements and substituting eqns (6b) and (6c) into the displacements, eqns (8a) and (8b) can be rewritten as

$$T_o = E_o \int_0^{t_o} \frac{du_o}{dx} dy' = E_o t_o \left(\frac{du_{co}}{dx} - \frac{t_o}{3G_o} \frac{d\tau_c}{dx} \right) \tag{9a}$$

and

$$T_i = 2E_i \int_0^{t_i/2} \frac{du_i}{dx} dy'' = E_i t_i \left(\frac{du_{ci}}{dx} + \frac{t_i}{6G_i} \frac{d\tau_c}{dx} \right). \tag{9b}$$

The adhesive shear strain (γ_c) is simply defined as

$$\gamma_c = \frac{1}{\eta}(u_{ci} - u_{co}). \tag{10}$$

The adhesive shear stress can be written as

$$\tau_c = \frac{G_c}{\eta}(u_{ci} - u_{co}). \tag{11}$$

By differentiating eqn (11) with respect to x, the equation becomes

$$\frac{d\tau_c}{dx} = \frac{G_c}{\eta} \left(\frac{du_{ci}}{dx} - \frac{du_{co}}{dx} \right). \tag{12}$$

Substituting eqns (9a) and (9b) into eqn (12) leads to

$$\frac{d\tau_c}{dx} = \frac{G_c}{\eta} \left[\frac{T_i}{E_i t_i} - \frac{T_o}{E_o t_o} - \left(\frac{t_i}{6G_i} - \frac{t_o}{3G_o} \right) \frac{d\tau_c}{dx} \right]. \tag{13}$$

By differentiating eqn (13) with respect to x and substituting eqns (2) and (3) into the differential equation, the equation becomes

$$\frac{d^2\tau_c}{dx^2} = \frac{G_c}{\eta} \left[\frac{2\tau_c}{E_i t_i} + \frac{\tau_c}{E_o t_o} - \left(\frac{t_i}{6G_i} + \frac{t_o}{3G_o} \right) \frac{d^2\tau_c}{dx^2} \right]. \tag{14}$$

By rearranging eqn (14), one obtains

$$\left[1 + \frac{G_c}{\eta} \left(\frac{t_i}{6G_i} + \frac{t_o}{3G_o} \right) \right] \frac{d^2\tau_c}{dx^2} = \frac{G_c}{\eta} \left(\frac{2}{E_i t_i} + \frac{1}{E_o t_o} \right) \tau_c \tag{15}$$

which governs the adhesive shear stress. It can be rewritten as

$$\frac{d^2\tau_c}{dx^2} - \beta^2 \tau_c = 0 \tag{16}$$

where

$$\beta^2 = \frac{\dfrac{G_c}{\eta}\left(\dfrac{2}{E_i t_i} + \dfrac{1}{E_o t_o}\right)}{\left[1 + \dfrac{G_c}{\eta}\left(\dfrac{t_i}{6G_i} + \dfrac{t_o}{3G_o}\right)\right]}. \tag{17}$$

The parameter β is redefined by two parameters λ (elongation parameter) and α (shear deformation parameter), as shown as

$$\beta^2 = \alpha^2 \lambda^2 \tag{18}$$

where

$$\lambda^2 = \frac{G_c}{\eta}\left(\frac{2}{E_i t_i} + \frac{1}{E_o t_o}\right), \tag{19}$$

$$\alpha^2 = \left[1 + \frac{G_c}{\eta}\left(\frac{t_i}{6G_i} + \frac{t_o}{3G_o}\right)\right]^{-1}. \tag{20}$$

The closed-form solution proposed by Volkersen/de Bruyne can be recovered by assuming that adherend shear deformations are zero, or that adherend shear moduli, G_i and G_0 are infinitely large, and $\alpha = 1$.

The general solution for the governing eqn (16) is

$$\tau_c = A \sinh(\beta x) + B \cosh(\beta x) \tag{21}$$

where A and B are constant coefficients determined from the boundary conditions. The boundary conditions for this double-lap joint are:

$$T_o = \frac{T}{2} = 2c\tau_{avg}, \quad T_i = 0 \quad \text{at } x = -c \tag{22a}$$

$$T_o = 0, \quad T_i = T = 4c\tau_{avg} \quad \text{at } x = c. \tag{22b}$$

The average shear stress along the entire bond line is:

$$\tau_{avg} = \frac{1}{2c}\int_{-c}^{c} \tau_c \, dx = \frac{T}{4c}. \tag{23}$$

Hence, the A and B are obtained as

$$B = \frac{\beta c \tau_{avg}}{\sinh(\beta c)} \tag{24}$$

and

$$A = \frac{\beta c \tau_{avg}}{\cosh(\beta c)}\left[\frac{1 - \dfrac{E_i t_i}{2E_o t_o}}{1 + \dfrac{E_i t_i}{2E_o t_o}}\right]. \tag{25}$$

Thus, the adhesive shear stress closed-form solution is given by eqn (21) with the constant coefficients A and B, from eqns (25) and (24), and the parameter β defined in eqn (17). The

maximum adhesive shear stress will occur at one end or the other (i.e. at $x = c$ or $x = -c$) depending upon the joint parameters.

Verification and parametric study

Two double-lap joints with graphite–epoxy laminated adherends were used in an evaluation of the theory. The joints had either unidirectional or quasi-isotropic composite adherends. For the unidirectional joint, a $[0]_{16}$ lay-up is used for the inner adherend and $[0]_8$ for the outer adherends. For the quasi-isotropic joint, a $[0/90/-45/45]_{2s}$ lay-up is for the inner adherend and $[0/90/-45/45]_s$ for the outer adherends. The geometrical parameters are:

$$2c = 12.7 \text{ mm}, \quad t_o = 1 \text{ mm}, \quad t_i = 2 \text{ mm}, \quad \text{and} \quad \eta = 0.15 \text{ mm}.$$

The relevant material properties are:

Adherends
unidirectional joint—$E_o = 137$ GPa, $G_o = 4.83$ GPa;
quasi-isotropic joint—$E_0 = 50$ GPa, $G_o = 3.80$ GPa.
Adhesive $G_c = 0.91$ GPa.

It is noted that G_o for the quasi-isotropic adherend is calculated by averaging G_o for all laminae, i.e. [0], [90], [−45] and [45], which are determined from the lamina three-dimensional (3-D) constitutive stiffness matrix. The value of the adhesive shear modulus G_c is an epoxy designed for EA9628NW and taken from the manufacturer's data.

The experimental analysis was performed using high-sensitivity moiré interferometry and the resulting data have been confirmed by comparing the data with two-dimensional (2-D) finite element results (Tsai *et al.*, 1996b). The experimental values of the adhesive shear strains, shown in Fig. 6, for these two joints are compared with the one-dimensional (1-D) Volkersen/de Bruyne solution. It is apparent that the Volkersen/de Bruyne solution over-estimates the non-uniformity of adhesive shear strain (stress) distribution and maximum adhesive shear strain (stress) for the unidirectional and quasi-isotropic double-lap joints. Analytical data from the present theory (TOM) are compared with those from

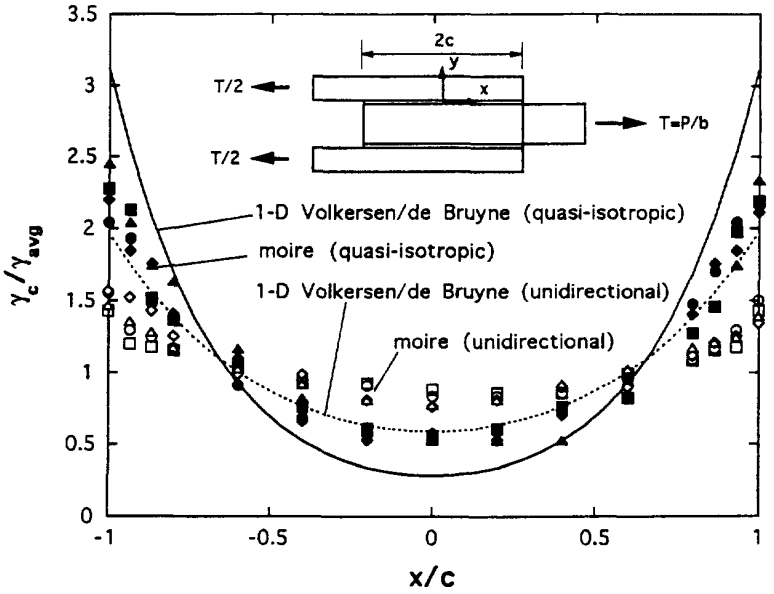

Fig. 6. Comparisons of moiré- and theory-determined normalized adhesive shear strain distributions for unidirectional and quasi-isotropic double-lap joints. (Note the theory is based on 1-D bar model of Volkersen/de Bruyne.)

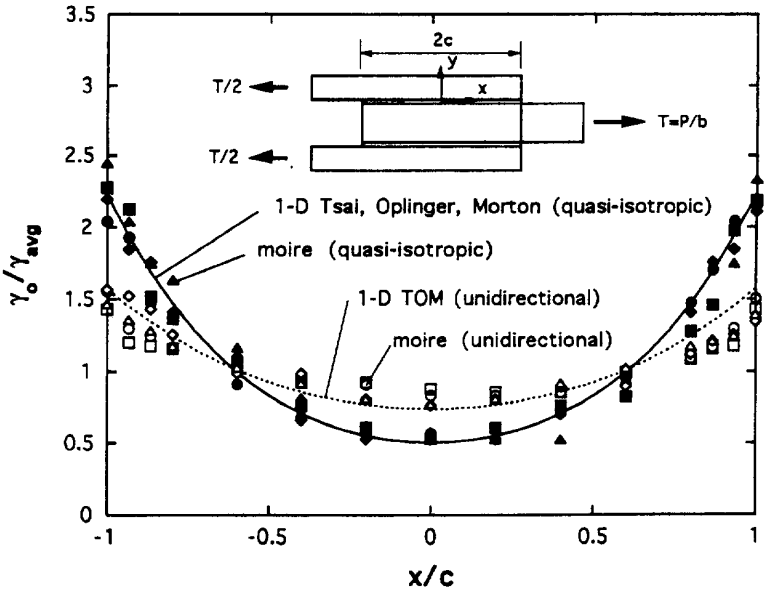

Fig. 7. Comparison of moiré- and improved theory-determined normalized adhesive shear strain distributions for unidirectional and quasi-isotropic double-lap joints. (Note the TOM represents the present 1-D bar model including the adherend shear deformations.)

the moiré experiment. These comparisons are presented in Fig. 7. The prediction from the present theory is more consistent with the experimental results for both unidirectional and quasi-isotropic double-lap joints, than those of Volkersen/de Bruyne. This implies that adherend shear deformation is an important factor influencing the adhesive shear stress distribution, especially for the joints with relatively low transverse shear stiffness such as with laminated fiber composite adherends.

The effect of adherend transverse shear stiffness on the maximum adhesive shear stress can be examined through a parametric study. For simplicity, only a balanced double-lap joint is considered. The geometry and material parameters for the balanced double-lap joint are taken as:

$$E_i = E_o = E, \quad G_i = G_o = G, \quad t_i = 2t_o = 2t. \tag{26a–c}$$

Substituting parameters into eqns (19) and (20), the elongation (λ) and shear deformation (α) parameters can be written as

$$\lambda = \sqrt{\frac{2G_c}{tE\eta}} \tag{27}$$

$$\alpha = \frac{1}{\sqrt{1+\dfrac{2G_c t}{3\eta G}}}. \tag{28}$$

Since the double joint is balanced, maximum adhesive shear will occur at both ends (at $x = c$ and $x = -c$) simultaneously. The maximum adhesive shear stress ($\max \tau_c$) is:

$$\max \tau_c = B\cosh(\beta c) = \beta c \tau_{avg} \coth(\beta c) = \alpha\lambda c \tau_{avg} \coth(\alpha\lambda c). \tag{29}$$

The ratio of the $\max \tau_c$ from the present analysis (TOM) to the $\max \tau_c$ determined from the Volkersen/de Bruyne analysis is given by

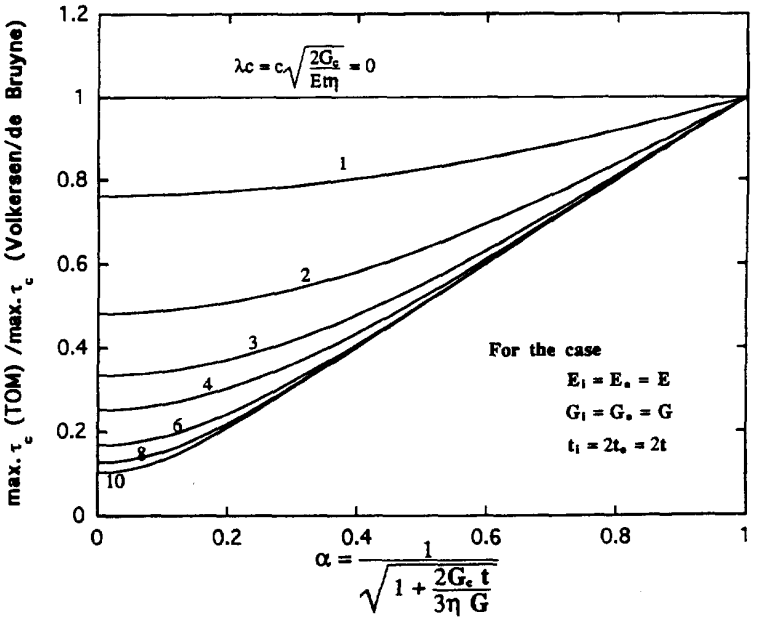

Fig. 8. The ratio of the maximum adhesive shear stresses from the present theory (TOM) to those from Volkersen/de Bruyne vs factor λc and α for the double-lap joints.

$$\frac{\max \tau_c(\text{TOM})}{\max \tau_c(\text{Volkersen/de Bruyne})} = \frac{\alpha \coth(\alpha \lambda c)}{\coth(\lambda c)} \tag{30}$$

and plotted in terms of parameters λc and α in Fig. 8. It is clear that decreasing α or increasing λc would result in a reduced normalized max τ_c (or decreasing the max adhesive shear stress which is provided by Volkersen/de Bruyne analysis). A reduced value of G (adherend shear modulus) would cause a decrease in α. Also an increase in the overlap length ($2c$) would produce an increase in λc, which results in a reduced value of normalized max τ_c. If the value of G is relatively large and the value of t is relatively small (so that $2G_c t/3\eta G \ll 1$), α would approach as one, and the normalized max τ_c would equal one. Then the adherend shear deformation can be neglected in the analysis and the Volkersen/de Bruyne analysis gives a reasonable prediction of adhesive shear stresses.

SINGLE-LAP JOINTS

Two formulations are proposed for single-lap joints. One is a 1-D bar formulation and the other is a 1-D beam formulation, according to the adherend deformation modeling used in the theories.

1-D bar formulation

The adherends are modeled as bars, which deform uniformly across the thickness of the adherends in the longitudinal direction (i.e. the longitudinal normal strain is constant through the thickness), and includes the simple shear deformation. The bar model neglects the effects of edge moment and shear force which are present in the single-lap joints (Goland and Reissner, 1944) (these effects will be addressed in the 1-D beam model). However, the bar model provides the easiest way to examine the mechanics of single-lap joints and the relevant parameters, especially for unbalanced joints. Furthermore, the 1-D bar model proposed by Volkersen has been used in theoretical approaches for stepped-lap joints and scarf joints (Hart-Smith, 1973c).

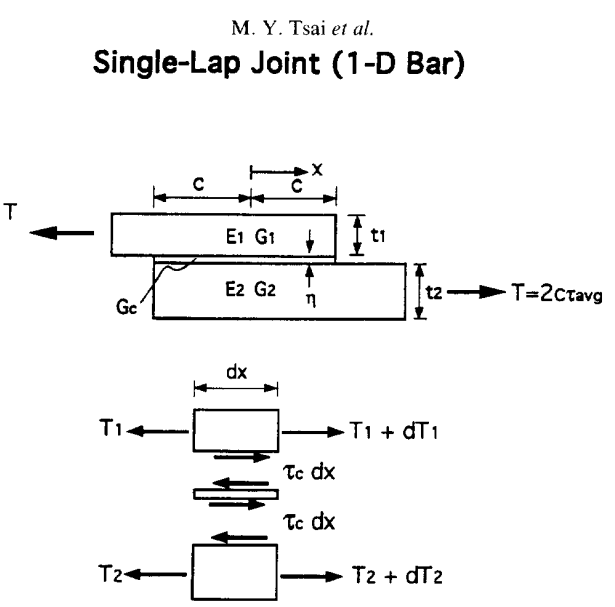

Fig. 9. Geometry and material parameters of the single-lap joint, and an elementary 1-D bar model.

The geometry and material parameters for the single-lap joint are shown in Fig. 9. The length of the overlap is $2c$. E_1, G_1 and t_1 represent elastic modulus, shear modulus, and thickness for the upper adherend, respectively, while E_2, G_2 and t_2 are the corresponding values for the lower adherend. T_1 and T_2 represent the longitudinal forces per unit width acting at the upper and lower adherends, respectively. T is an applied force per unit width. Assuming a linear adherend shear stress distribution through the thickness of adherends, the adhesive shear stress τ_c is obtained as (Appendix A):

$$\tau_c = A\sinh(\beta x) + B\cosh(\beta x) \tag{31}$$

where

$$A = \frac{\beta c \tau_{avg}}{\cosh(\beta c)} \left[\frac{1 - \dfrac{E_2 t_2}{E_1 t_1}}{1 + \dfrac{E_2 t_2}{E_1 t_1}} \right], \tag{32}$$

$$B = \frac{\beta c \tau_{avg}}{\sinh(\beta c)}, \tag{33}$$

and

$$\beta^2 = \frac{\dfrac{G_c}{\eta}\left(\dfrac{1}{E_1 t_1} + \dfrac{1}{E_2 t_2}\right)}{\left[1 + \dfrac{G_c}{\eta}\left(\dfrac{t_1}{3G_1} + \dfrac{t_2}{3G_2}\right)\right]}. \tag{34}$$

The average adhesive shear stress τ_{avg} is equal to $T/2c$. The parameter β can be written in terms of λ (elongation parameter) and α (shear deformation parameter) as

$$\beta^2 = \alpha^2 \lambda^2 \tag{35}$$

where

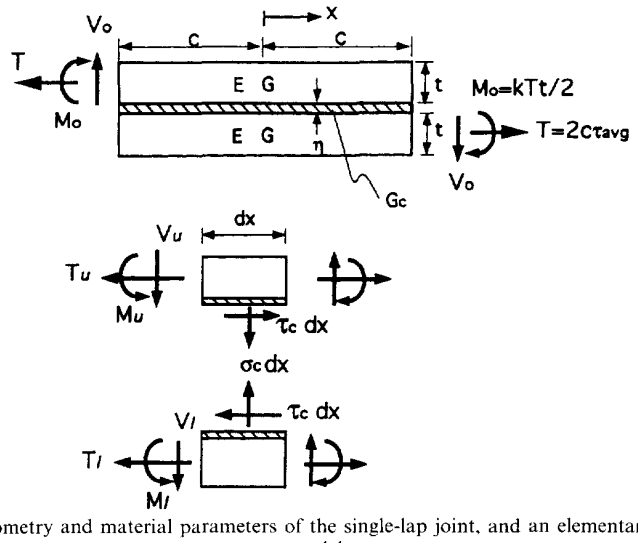

Fig. 10. Geometry and material parameters of the single-lap joint, and an elementary 1-D beam model.

$$\lambda^2 = \frac{G_c}{\eta}\left(\frac{1}{E_1 t_1} + \frac{1}{E_2 t_2}\right),$$

$$\alpha^2 = \left[1 + \frac{G_c}{\eta}\left(\frac{t_1}{3G_1} + \frac{t_2}{3G_2}\right)\right]^{-1}. \tag{36a,b}$$

Note that when $\alpha = 1$ Volkersen's solution is obtained, and the effect of the adherend shear deformation is negligible.

1-D beam formulation

The configuration of the single-lap joint is shown in Fig. 10. Balanced joints are analyzed in this study. E, G and t represent adherend longitudinal elastic modulus, transverse shear modulus, and thickness of the adherend, respectively, while G_c and η are shear modulus and thickness for the adhesive layer. M_o and V_o are edge moment and shear force per unit width acting at the end of the overlap. T is the longitudinal applied force per unit width.

In the Goland the Reissner solution, the adherends are modeled as beams. That is, the transverse normal strain and shear strain in the adherends are negligibly small compared with the corresponding strains in the adhesive layer. However, if the transverse normal strain and shear strain in the adherends are not small, both components have to be taken into account in the analysis. Thus, a 2-D analysis has to be employed. A closed-form solution based on 2-D elasticity analysis is very complex. Instead, a simple solution based on 1-D beam analysis, but including the shear deformation of the adherends is proposed. The adherend shear deformation is assumed similar to the shear deformation addressed in the double-lap joints. Since the adherend shear deformations affect only the adhesive shear stress distributions and not the peel stress, the adhesive stress analysis will be confined to the shear stress determination.

The detailed analysis is described in Appendix B. The solution of the normalized adhesive shear stress τ_c is

$$\frac{\tau_c}{\tau_{avg}} = \frac{1}{4}\left[\frac{\beta c}{t}(1+3k)\frac{\cosh\left(\frac{\beta c}{t}\frac{x}{c}\right)}{\sinh\frac{\beta c}{t}} + 3(1-k)\right] \tag{37}$$

where $k = 2M_o/Tt$, $\tau_{avg} = T/2c$ and

$$\beta^2 = \frac{8tG_c}{E\eta}\left(\frac{1}{1+\frac{2G_c t}{3\eta G}}\right). \tag{38}$$

The parameter β can be redefined by two parameters λ (longitudinal deformation parameter) and α (shear deformation parameter):

$$\beta^2 = \alpha^2\lambda^2 \tag{39}$$

where

$$\lambda^2 = \frac{8G_c t}{E\eta} = \frac{4E_c t}{E\eta(1+v_c)} \tag{40}$$

$$\alpha^2 = \frac{1}{1+\frac{2G_c t}{3\eta G}}. \tag{41}$$

Note that for the Goland and Reissner solution, $\alpha = 1$. That is $2G_c t/3\eta G \ll 1$.

Verification and parametric study

Two cases are used to verify the 1-D bar and beam models. One case is a balanced thick-adherend single-lap joint subjected only longitudinal force. The other is the same single-lap joint, but subjected to a longitudinal force and edge moment (M_o). For the geometry of this thick-adherend single-lap joint, the length of the overlap ($2c$) is 9.53 mm. The thickness of the adherend is 9.53 mm. The thickness of the adhesive (η) is 0.152 mm. The adherends are aluminum ($E = 70$ GPa, $G = 26.3$ GPa) while the adhesive is epoxy ($E_c = 2.17$ GPa, $G_c = 0.83$ GPa). For the first case, the normalized adhesive shear distributions along the half of the bond line are shown in Fig. 11. It is shown that the Volkersen solution is very close to the Goland and Reissner solution with zero edge moment ($k = 0$). Furthermore, the present solutions, Volkersen's and Goland and Reissner's solutions with adherend shear deformation, are very consistent with each other. This consistency suggests the validity of these two models. It is also apparent that the adherend shear deformation reduces the adhesive shear stress concentration and thus render the adhesive shear distribution more uniform. For the other case, the edge moment ($M_o = tT/2$) is included. This case is more realistic than the previous case. The comparisons of adhesive shear distributions are shown in Fig. 12 which contains the results of the moiré experiment (Tsai *et al.*, 1996a), 2-D finite element analysis, Goland and Reissner's theoretical solution and the present analysis (modified Goland and Reissner's solutions with adherend shear deformation). It is apparent that the moiré experimental result is consistent with that from the 2-D finite element analysis, but not Goland and Reissner's prediction. However, the present analysis with including adherend shear deformation provides a better prediction of adhesive shear stress distribution than the original Goland and Reissner solution.

For the 1-D beam model, the maximum adhesive shear stress will occur at both ends of the overlap (at $x = c$ and $-c$) for balanced single-lap joints. From eqn (37), the normalized maximum adhesive shear is

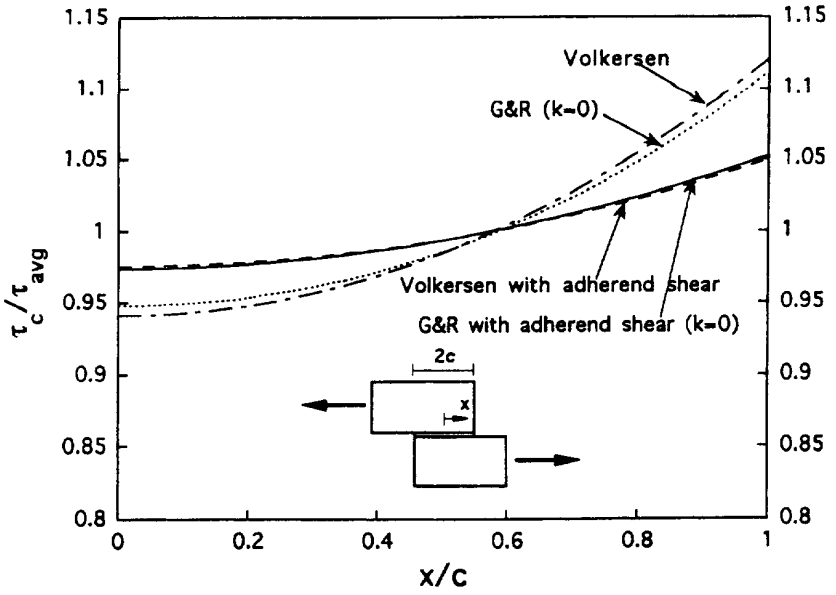

Fig. 11. Normalized adhesive shear stress distributions of thick-adherend single-lap joint predicted by 1-D bar model (Volkersen), 1-D beam model (Goland and Reissner), the present 1-D bar model (Volkersen with adherend shear) and the present 1-D beam model (Goland and Reissner with adherend shear).

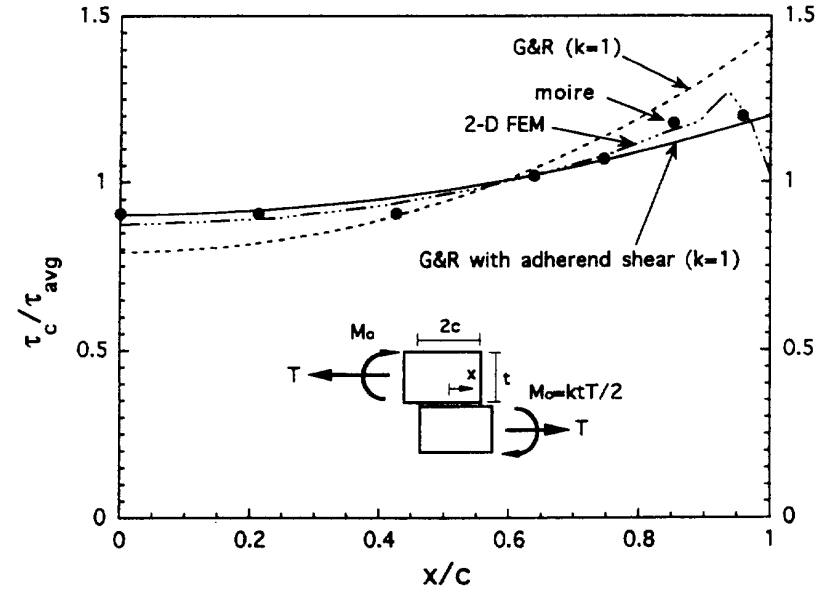

Fig. 12. Normalized adhesive shear stress distributions of thick-adherend single-lap joint with the edge moment (M_o), determined from the moiré experiment, 2-D finite element model (FEM), 1-D beam model (Goland and Reissner), and the present 1-D beam model (Goland and Reissner with adherend shear).

$$\frac{\max \tau_c}{\tau_{avg}} = \frac{1}{4}\left[\frac{\beta c}{t}(1+3k)\coth\frac{\beta c}{t} + 3(1-k)\right] \tag{42}$$

where $\beta = \alpha\lambda$. In order to understand the effect of adherend shear deformations on the maximum adhesive shear stress, the maximum adhesive shear determined from the present analysis (TOM) is normalized by that obtained from the Goland and Reissner analysis which neglects the adherend shear deformation. That is:

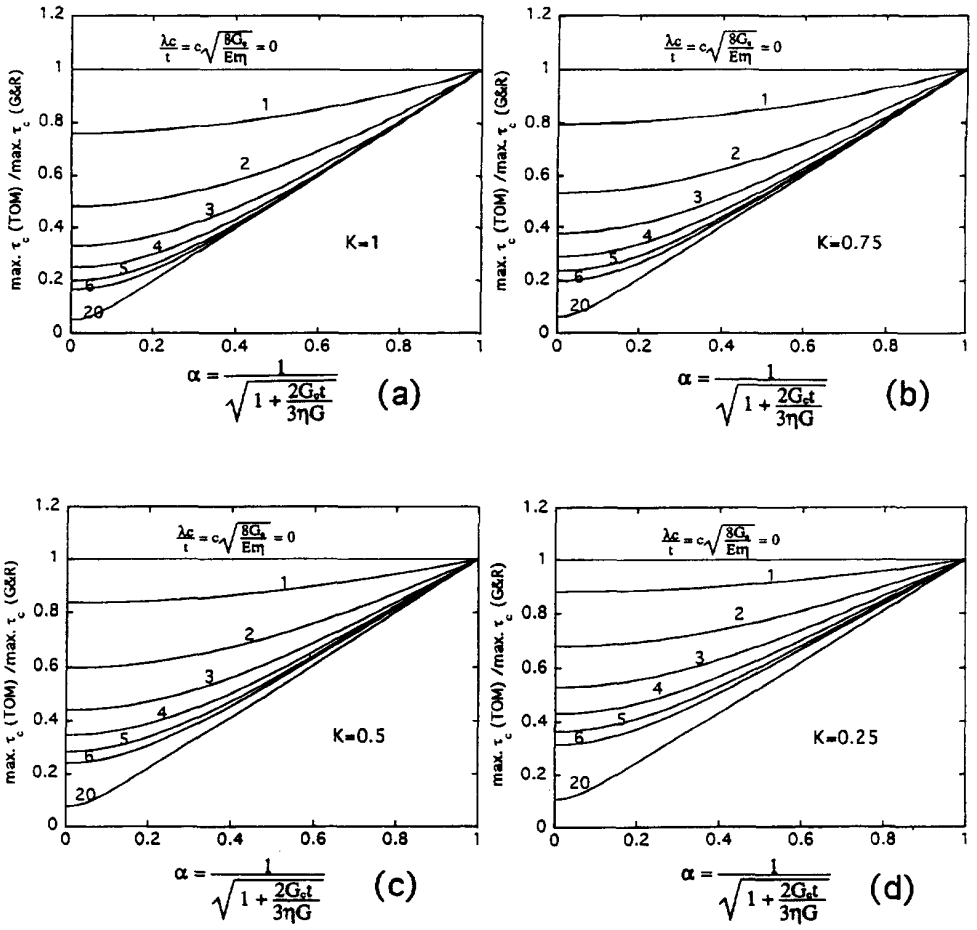

Fig. 13. The ratio of the maximum adhesive shear stresses from the present theory (TOM) to those from Goland and Reissner vs factor $\lambda c/t$ and α for the single-lap joints with edge moment factor: (a) $k = 1$; (b) $k = 0.75$; (c) $k = 0.5$; and (d) $k = 0.25$.

$$\frac{\max \tau_c(\text{TOM})}{\max \tau_c(\text{G\&R})} = \frac{\dfrac{\alpha\lambda c}{t}(1+3k)\coth\left(\dfrac{\alpha\lambda c}{t}\right)+3(1-k)}{\dfrac{\lambda c}{t}(1+3k)\coth\left(\dfrac{\lambda c}{t}\right)+3(1-k)}. \tag{43}$$

Equation (43) is plotted against α and $\lambda c/t$ and shown in Fig. 13 for different values of k. The results indicate that the maximum adhesive shear stress is insensitive to the adherend shear deformation (parameter α), as $\lambda c/t$ approaches to zero or equals zero. It is also apparent that, as the value of $\lambda c/t$ increases, the normalized maximum adhesive shear stress decreases for given α and k. This implies the longer the overlap, the greater the effect of adherend shear deformation. Furthermore, decreasing α results in decreasing the normalized maximum shear stress if the values of $\lambda c/t$ and k are fixed. That means the smaller the α, the higher the effect of adherend shear deformation. The relatively low adherend shear modulus (G) would cause the low value of α. The magnitude of the edge moment (related to the value of k) also influences the maximum adhesive shear stress.

CONCLUSIONS

An improvement to the classical theoretical solutions for adhesive lap joints (including double- and single-lap joints) has been proposed in the present study. The adherend shear

deformations have been included in the theoretical analyses by assuming a linear shear stress (strain) through the thickness of the adherends. The assumptions and improved solutions have been validated by comparing with the experimental and numerical solutions. It has been shown that the improved theoretical solutions provide a better prediction than the classical solutions, especially for the adherends with relatively low transverse shear stiffness (for example, in the case of laminated composite adherends). The classical solutions which neglect the adherend shear deformations over-estimate the non-uniformity of the adhesive shear distributions and maximum adhesive shear stress (strain). It is also shown that the classical solutions can be recovered from the improved solutions, and the improved Volkersen's solution can be recovered from the improved Goland and Reissner's solution. The critical parameter related to adherend shear deformation, which affect adhesive shear stress (strain) distribution, have been identified.

Acknowledgement—The financial support from the Federal Aviation Administration under the contract USDOT/FAA 93-G-064 is greatly appreciated.

REFERENCES

de Bruyne, N. A. (1944) The strength of glued joints. *Aircraft Engineering* **16,** 115–118.
Delale, F., Erdogan, F. and Aydinoglu, M. N. (1981) Stresses in adhesively bonded joints : a closed-form solution. *Journal of Composite Materials* **15,** 249–271.
Goland, M. and Reissner, E. (1944) The stresses in cemented joints. *Journal of Applied Mechanics* **11,** A17–A27.
Hart-Smith, L. J. (1973a) Adhesive-bonded single-lap joints. NASA, CR-112236.
Hart-Smith, L. J. (1973b) Adhesive-bonded double-lap joints. NASA, CR-112235.
Hart-Smith, L. J. (1973c) Adhesive-bonded scarf and stepped-lap joints. NASA, CR-112237.
Lin, C. C. and Lin, Y. S. (1993) A finite element model of single-lap adhesive joints. *International Journal of Solids and Structures* **30**(12), 1679–1692.
Oplinger, D. W. (1994) Effects of adherend deflections in single lap joints. *International Journal of Solids and Structures* **31,** 2565-2587.
Suhir, E. (1986) Stresses in bimetal thermostats. *Journal of Applied Mechanics* **53**(3), 657–660.
Suhir, E. (1989) Interfacial stresses in bi-metal thermostats. *Journal of Applied Mechanics* **56,** 595–600.
Suhir, E. (1994) Approximate evaluation of the interfacial shearing stress in cylindrical double lap shear joints with application to dual-coated optical fibers. *International Journal of Solids and Structures* **31**(23), 3261–3283.
Tsai, M. Y. and Morton, J. (1994) An evaluation of analytical and numerical solutions to the single-lap joint. *International Journal of Solids and Structures* **31**(18), 2537–2563.
Tsai, M. Y. and Morton, J. (1995) An experimental investigation of nonlinear deformations in single-lap joints. *Mechanics of Material* **20,** 183–194.
Tsai, M. Y., Morton, J., Kreiger, R. B. and Oplinger, D. W. (1996a) Experimental investigation of the thick-adherend lap shear test. *Journal of Advanced Materials*, **April,** 28–36.
Tsai, M. Y., Morton, J. and Oplinger, D. W. (1996b) Deformation and stress analyses of double-lap adhesive joints with laminated composite adherends. *The SEM VIII International Congress*, Nashville, Tennessee.
Volkersen, O. (1938) Die Niektraftverteilung in Zugbeanspruchten mit Konstanten Laschenquerschritten. *Luftfahrtforschung* **15,** 41–47.

APPENDICES

Appendix A (improved Volkersen's solution)

The elementary model of a single-lap joint is demonstrated in Fig. 9. Force equilibrium equations in the x-direction for adherend elements are expressed as

$$\frac{dT_1}{dx} + \tau_c = 0, \tag{A1}$$

$$\frac{dT_2}{dx} - \tau_c = 0 \tag{A2}$$

where τ_c is adhesive shear stress. Adherend shear deformations are incorporated in this analyses. A linear shear stress (strain) distribution through the thickness of the adherend is assumed. Thus, the adherend shear τ_1 for the upper adherend and τ_2 for the lower adherend can be expressed as:

$$\tau_1 = \frac{\tau_c}{t_1} y' \tag{A3}$$

and

$$\tau_2 = \tau_c\left(1-\frac{y''}{t_2}\right) \tag{A4}$$

where y' (y'') is a local coordinate system with the origin at the top surface of the upper (lower) adherend. The eqns (A3) and (A4) are based on zero shear stresses at the top surface of the upper adherend (i.e. at $y' = 0$) and at the bottom surface of the lower adherend (i.e. at $y'' = t_2$), and $\tau_1 = \tau_c$ at $y' = t_1$ and $\tau_2 = \tau_c$ at $y'' = 0$. The adherend shear strain γ_1 for the upper adherend and γ_2 for the lower adherend are written as

$$\gamma_1 = \frac{\tau_c}{G_1 t_1} y' \tag{A5}$$

and

$$\gamma_2 = \frac{\tau_c}{G_2}\left(1-\frac{y''}{t_2}\right). \tag{A6}$$

The longitudinal displacement functions u_1 for the upper adherend and u_2 for the lower adherend are given by

$$u_1(y') = u_{1s} + \int_0^{y'} \gamma_1(\hat{y}')\,\mathrm{d}\hat{y}' = u_{1s} + \frac{\tau_c}{2G_1 t_1} y'^2 \tag{A7}$$

and

$$u_2(y'') = u_{c2} + \int_0^{y''} \gamma_2(\hat{y}'')\,\mathrm{d}\hat{y}'' = u_{c2} + \frac{\tau_c}{G_2}\left(y'' - \frac{y''^2}{2t_2}\right) \tag{A8}$$

where u_{1s} represents the displacement at the top surface of the upper adherend and u_{c2} is the adhesive displacement at the interface between the adhesive and lower adherend.

Note that due to the perfect bonding of the joints the displacements are continuous at the interfaces between the adhesive and adherends. As a result, the u_{c2} should be equivalent to the lower adherend displacement at the interface and u_{c1} (the adhesive displacement at the interface between the adhesive and upper adherend) should be the same as the upper adherend displacement at the interface. Based on eqn (A7) the u_{c1} can be expressed as

$$u_{c1} = u_1(y' = t_1) = u_{1s} + \frac{\tau_c t_1}{2G_1}. \tag{A9}$$

Using eqn (A9), eqn (A7) can be rewritten as

$$u_1(y') = u_{c1} + \frac{\tau_c}{2G_1 t_1} y'^2 - \frac{\tau_c t_1}{2G_1}. \tag{A10}$$

The longitudinal resultant forces, T_1 and T_2 for the upper and lower adherends, respectively, are:

$$T_1 = \int_0^{t_1} \sigma_1(y')\,\mathrm{d}y' \tag{A11}$$

and

$$T_2 \int_0^{t_2} \sigma_2(y'')\,\mathrm{d}y'' \tag{A12}$$

where σ_1 and σ_2 are longitudinal normal stresses for the upper and lower adherends, respectively. By changing these stresses into functions of the displacements and substituting equations (A8) and (A10) into the displacements, eqns (A11) and (A12) can be rewritten as

$$T_1 = E_1 \int_0^{t_1} \frac{\mathrm{d}u_1}{\mathrm{d}x}\,\mathrm{d}y' = E_1 t_1\left(\frac{\mathrm{d}u_{c1}}{\mathrm{d}x} - \frac{t_1}{3G_1}\frac{\mathrm{d}\tau_c}{\mathrm{d}x}\right) \tag{A13}$$

and

$$T_2 = E_2 \int_0^{t_2} \frac{\mathrm{d}u_2}{\mathrm{d}x}\,\mathrm{d}y'' = E_2 t_2\left(\frac{\mathrm{d}u_{c2}}{\mathrm{d}x} + \frac{t_2}{3G_2}\frac{\mathrm{d}\tau_c}{\mathrm{d}x}\right). \tag{A14}$$

The adhesive shear strain (γ_c) is simply defined as

$$\gamma_c = \frac{1}{\eta}(u_{c2} - u_{c1}). \tag{A15}$$

The adhesive shear stress can be written as

$$\tau_c = \frac{G_c}{\eta}(u_{c2} - u_{c1}). \tag{A16}$$

By differentiating eqn (A16) with respect to x, one obtains

$$\frac{d\tau_c}{dx} = \frac{G_c}{\eta}\left(\frac{du_{c2}}{dx} - \frac{du_{c1}}{dx}\right). \tag{A17}$$

Substituting eqns (A13) and (A14) into (A17) leads to

$$\frac{d\tau_c}{dx} = \frac{G_c}{\eta}\left[\frac{T_2}{E_2 t_2} - \frac{T_1}{E_1 t_1} - \left(\frac{t_2}{3G_2} + \frac{t_1}{3G_1}\right)\frac{d\tau_c}{dx}\right]. \tag{A18}$$

By differentiating eqn (A18) with respect to x and substituting eqns (A1) and (A2) into the differential equation, the equation becomes

$$\frac{d^2\tau_c}{dx^2} = \frac{G_c}{\eta}\left[\frac{\tau_c}{E_2 t_2} + \frac{\tau_c}{E_1 t_1} - \left(\frac{t_2}{3G_2} + \frac{t_1}{3G_1}\right)\frac{d^2\tau_c}{dx^2}\right]. \tag{A19}$$

The governing eqn (A19) can be rewritten as

$$\frac{d^2\tau_c}{dx^2} - \beta^2\tau_c = 0 \tag{A20}$$

where

$$\beta^2 = \frac{\frac{G_c}{\eta}\left(\frac{1}{E_2 t_2} + \frac{1}{E_1 t_1}\right)}{\left[1 + \frac{G_c}{\eta}\left(\frac{t_2}{3G_2} + \frac{t_1}{3G_1}\right)\right]}. \tag{A21}$$

The parameter β can be redefined as

$$\beta^2 = \alpha^2\lambda^2 \tag{A22}$$

where the parameter λ (elongation parameter) and α (shear deformation parameter) are

$$\lambda^2 = \frac{G_c}{\eta}\left(\frac{1}{E_2 t_2} + \frac{1}{E_1 t_1}\right), \tag{A23}$$

$$\alpha^2 = \left[1 + \frac{G_c}{\eta}\left(\frac{t_2}{3G_2} + \frac{t_1}{3G_1}\right)\right]^{-1}. \tag{A24}$$

The solution for the governing eqn (A20) is

$$t_c = A\sinh(\beta x) + B\cosh(\beta x) \tag{A25}$$

where A and B are constant coefficients which can be determined from the given boundary conditions. The boundary conditions for this single-lap joint are:

$$T_1 = T = 2c\tau_{avg}, \quad T_2 = 0 \quad \text{at } x = -c, \tag{A26}$$

$$T_1 = 0, \quad T_2 = T = 2c\tau_{avg} \quad \text{at } x = c. \tag{A27}$$

The integration of adhesive shear stresses along the entire bond line is equivalent to T. That is:

$$T = 2c\tau_{avg} = \int_{-c}^{c} \tau_c \, dx. \tag{A28}$$

The A and B are obtained as

$$B = \frac{\beta c \tau_{avg}}{\sinh(\beta c)}, \tag{A29}$$

$$A = \frac{\beta c \tau_{avg}}{\cosh(\beta c)} \left[\frac{1 - \dfrac{E_2 t_2}{E_1 t_1}}{1 + \dfrac{E_2 t_2}{E_1 t_1}} \right]. \tag{A30}$$

Appendix B (improved Goland and Reissner's solution)

Following the adhesive stress analysis in Goland and Reissner Part III solution, the elementary model is shown in Fig. 10. Only adhesive shear formulation is considered here, since the adhesive peel stress is not affected by adherend shear deformation based on the Goland and Reissner 1-D beam model. The derivations are as follows.

Moment equilibrium equations for the basic elements of the upper and lower adherends are given by

$$\frac{dM_u}{dx} - V_u - \tau_c \frac{t}{2} = 0, \tag{B1}$$

$$\frac{dM_l}{dx} - V_l - \tau_c \frac{t}{2} = 0 \tag{B2}$$

where M_u (M_l) and V_u (V_l) are the upper-adherend (lower-adherend) moment and shear per unit width, respectively. Force equilibrium equations in the longitudinal direction for both elements can be written as

$$\frac{dT_u}{dx} + \tau_c = 0, \tag{B3}$$

$$\frac{dT_l}{dx} - \tau_c = 0 \tag{B4}$$

where T_u and T_l are longitudinal forces per unit width for the upper and lower adherends, respectively. Force equilibrium equations in the transverse direction for both elements are given by

$$\frac{dV_u}{dx} - \sigma_c = 0 \tag{B5}$$

$$\frac{dV_l}{dx} + \sigma_c = 0 \tag{B6}$$

where σ_c is the adhesive peel (transverse normal) stress. Shear deformations of the adherends are incorporated in this analyses. A linear shear stress (strain) distribution through the thickness of the adherend is assumed. Thus, the adherend shear τ_u for the upper adherend and τ_l for the lower adherend can be expressed as

$$\tau_u = \frac{\tau_c}{t} y' \tag{B7}$$

and

$$\tau_l = \tau_c \left(1 - \frac{y''}{t}\right) \tag{B8}$$

where y' (y'') is a local coordinate system with the origin at the top surface of the upper (lower) adherend. The eqns (B7) and (B8) are based on zero shear stresses at the top surface of the upper adherend (i.e. at $y' = 0$) and at the bottom surface of the lower adherend (i.e. at $y'' = t$), and $\tau_u = \tau_c$ at $y' = t$ and $\tau_l = \tau_c$ at $y'' = 0$. Then with a linear material constitutive relationship the adherend shear strain γ_u for the upper adherend and γ_l for the lower adherend are written as

$$\gamma_u = \frac{\tau_c}{Gt} y' \tag{B9}$$

and

$$\gamma_l = \frac{\tau_c}{G} \left(1 - \frac{y''}{t}\right). \tag{B10}$$

The longitudinal displacement functions u_u^I for the upper adherend and u_l^I for the lower adherend, due to the longitudinal forces, are given by

$$u_u^T(y') = u_{cu}^T - \frac{\tau_c t}{2G} + \int_0^{y'} \gamma_u(\hat{y}')\,d\hat{y}' = u_{cu}^T - \frac{\tau_c t}{2G} + \frac{\tau_c}{2Gt}y'^2 \tag{B11}$$

and

$$u_l^T(y'') = u_{cl}^T + \int_0^{y''} \gamma_l(\hat{y}'')\,d\hat{y}'' = u_{cl}^T + \frac{\tau_c}{G}\left(y'' - \frac{y''^2}{2t}\right) \tag{B12}$$

where u_{cu}^T (u_{cl}^T) represents the longitudinal force-induced adhesive displacement at the interface between the upper (lower) adherend and the adhesive. The longitudinal resultant forces, T_u and T_l for the upper and lower adherends, respectively, are

$$T_u = \int_0^t \sigma_u^T(y')\,dy' \tag{B13}$$

and

$$T_l = \int_0^t \sigma_l^T(y'')\,dy'' \tag{B14}$$

where σ_u^T and σ_l^T are longitudinal normal stresses for the upper and lower adherends, respectively. By changing these stresses into functions of the displacements and substituting eqns (B11) and (B12) into the displacements, eqns (B13) and (B14) can be rewritten as

$$T_u = E\int_0^t \frac{du_u^T}{dx}dy' = Et\left(\frac{du_{cu}^T}{dx} - \frac{t}{3G}\frac{d\tau_c}{dx}\right) \tag{B15}$$

and

$$T_l = E\int_0^t \frac{du_l^T}{dx}dy'' = Et\left(\frac{du_{cl}^T}{dx} + \frac{t}{3G}\frac{d\tau_c}{dx}\right). \tag{B16}$$

The adhesive shear strain (γ_c) is simply defined as

$$\gamma_c = \frac{1}{\eta}(u_{cl} - u_{cu}) \tag{B17}$$

where u_{cu} (u_{cl}) represents the total displacement at the interface between the upper (lower) adherent and the adhesive. These total displacements can be expressed as

$$u_{cu} = u_{cu}^T - u_{cu}^M \tag{B18}$$

and

$$u_{cl} = u_{cl}^T + u_{cl}^M \tag{B19}$$

where u_{cu}^M (u_{cl}^M) represents the moment-induced displacement at the interface between the upper (lower) adherend and the adhesive. Assuming no effect of the adherend shear deformation on the adherend moment, these moment-induced strains can be simply written as

$$\frac{du_{cu}^M}{dx} = \frac{M_u}{EI_u}\frac{t}{2} = \frac{6M_u}{Et^2} \tag{B20}$$

and

$$\frac{du_{cl}^M}{dx} = \frac{M_l}{EI_l}\frac{t}{2} = \frac{6M_l}{Et^2} \tag{B21}$$

where I_u (I_l) are the moment of initia for the upper (lower) adherend. The adhesive shear stress can be written as

$$\tau_c = \frac{G_c}{\eta}(u_{cl} - u_{cu}). \tag{B22}$$

By differentiating eqn (B22) with respect to x, the equation becomes

$$\frac{d\tau_c}{dx} = \frac{G_c}{\eta}\left(\frac{du_{cl}}{dx} - \frac{du_{cu}}{dx}\right). \tag{B23}$$

Using eqns (B15), (B16) and (B18)–(B21), eqn (B23) leads to

$$\frac{d\tau_c}{dx} = \frac{G_c}{\eta}\left(\frac{T_l}{Et} - \frac{T_u}{Et} + 6\frac{M_u + M_l}{Et^2} - \frac{2t\,d\tau_c}{3G\,dx}\right). \tag{B24}$$

Differentiating eqn (B24) with respect to x and substituting eqns (B1)–(B4) into this equation, the differential equation becomes

$$\left(\frac{\eta}{G_c} + \frac{2t}{3G}\right)\frac{d^2\tau_c}{dx^2} = \frac{1}{E}\left(\frac{2\tau_c}{t} + \frac{6\tau_c}{t} + 6\frac{V_u + V_l}{t^2}\right). \tag{B25}$$

Differentiating eqn (B25) with respect to x and using eqns (B5) and (B6), eqn (B25) becomes

$$\left(\frac{\eta}{G_c} + \frac{2t}{3G}\right)\frac{d^3\tau_c}{dx^3} = \left(\frac{8}{Et}\right)\frac{d\tau_c}{dx}. \tag{B26}$$

Equation (B26) can be rewritten as

$$\frac{d^3\tau_c}{dx^3} - \frac{\beta^2}{t^2}\frac{d\tau_c}{dx} = 0 \tag{B27}$$

where

$$\beta^2 = \frac{8tG_c}{E\eta}\left(\frac{1}{1 + \dfrac{2G_c t}{3\eta G}}\right). \tag{B28}$$

The boundary conditions are:
at $x = c$

$$M_u = T_u = V_u = 0$$
$$M_l = M_o, \quad T_l = T, \quad V_l = -V_o;$$

at $x = -c$

$$M_l = T_l = V_l = 0$$
$$M_u = -M_o, \quad T_u = T, \quad V_u = -V_o.$$

Referring to eqn (B24) the above boundary conditions can be rewritten as:

at $x = c$,

$$\frac{d\tau_c}{dx} = \frac{1}{Et\left(\dfrac{\eta}{G_c} + \dfrac{2t}{3G}\right)}\left(T + 6\frac{M_o}{t}\right); \tag{B29}$$

at $x = c$,

$$\frac{d\tau_c}{dx} = -\frac{1}{Et\left(\dfrac{\eta}{G_c} + \dfrac{2t}{3G}\right)}\left(T + 6\frac{M_o}{t}\right). \tag{B30}$$

The equilibrium condition is given by

$$\int_{-c}^{c} \tau_c \, dx - T = 0. \tag{B31}$$

Based on the governing eqn (B27) and boundary conditions (B29), (B30) and (B31), the adhesive shear can be solved and written as

$$\frac{\tau_c}{\tau_{avg}} = \frac{1}{4}\left[\frac{\beta c}{t}(1+3k)\frac{\cos\left(\frac{\beta c}{t}\frac{x}{c}\right)}{\sinh\frac{\beta c}{t}} + 3(1-k)\right] \tag{B32}$$

where $k = 2M_0/Tt$, $\tau_{avg} = T/2c$ and

$$\beta^2 = \frac{8tG_c}{E\eta}\left(\frac{1}{1+\frac{2G_c t}{3\eta G}}\right). \tag{B33}$$